

The signatures of the new particles h_2 and $Z_{\mu\tau}$ at e-p colliders in the $U(1)_{L_\mu-L_\tau}$ model

Jin-Xin Hou ^{*}, Chong-Xing Yue [†]

Department of Physics, Liaoning Normal University, Dalian 116029, China

Abstract

Considering the superior performances of the two future e-p colliders, LHeC and FCC-eh, we discuss the feasibility of detecting the additional neutral scalar h_2 and the light gauge boson $Z_{\mu\tau}$, which are predicted by the $U(1)_{L_\mu-L_\tau}$ model. Taking into account the experimental constraints on the relevant free parameters, we consider all possible production channels of h_2 and $Z_{\mu\tau}$ at e-p colliders and further investigate their observability through the optimal channels in the case of the beam polarization $P(e^-) = -0.8$. We find that the signal significance above 5σ of h_2 as well as $Z_{\mu\tau}$ detecting can be achieved via $e^-p \rightarrow e^-j h_2 (\rightarrow Z_{\mu\tau} Z_{\mu\tau}) \rightarrow e^-j + \cancel{E}_T$ process and a 5σ sensitivity of $Z_{\mu\tau}$ detecting can be gained via $e^-p \rightarrow e^-j h_1 (\rightarrow Z_{\mu\tau} Z_{\mu\tau}) \rightarrow e^-j + \cancel{E}_T$ process at e-p colliders with appropriate parameter values and a designed integrated luminosity.

I. Introduction

Establishment of the standard model (SM) of elementary particle physics provides a very successful description of existing experiments at the highest energy currently available at colliders and explains the fundamental interactions of nature over the wide range of energy scale from eV to TeV. Discovery of the 125 GeV Higgs boson at the Large Hadron Collider (LHC) in 2012 [1, 2], which ushered in a new era of probing the mechanism of spontaneous symmetry breaking and thus mass generation via the Higgs-Englert-Brout mechanism, once again proves the correctness of the SM. However, so far the SM still has certain limitations. Some experimental facts have been plaguing people, and there is an urgent need to extend the SM. For instance, the sub-eV masses and peculiar mixing pattern of neutrinos [3, 4], the muon $(g-2)$ anomalous magnetic moment [5], the exploration of dark matter (DM) [6] and dark energy [7, 8], the baryon asymmetry of the Universe and so on. In addition to this, discovery of Higgs boson provides an outstanding portal to new physics (NP) beyond the SM simultaneously. Precision measurements of the Higgs boson properties are also one of the most important and pressing tasks of high-energy particle physics of our time due to its possible role as portal to beyond the SM (BSM) sectors [9–13].

In order to address the above issues, there are many well motivated extensions of the SM like SUSY [14–17], two Higgs doublet model [18–23], extension of the SM with an extra $U(1)$ gauge group [24–27] and many more. In this work, we have considered the gauged $U(1)_{L_\mu-L_\tau}$ extension of the SM due to its relatively simple theoretical structure and background free environment, which has a complete gauge group $SU(3)_C \times SU(2)_L \times U(1)_Y \times U(1)_{L_\mu-L_\tau}$ and is called the $U(1)_{L_\mu-L_\tau}$ model [28–35]. One of the advantages of

^{*}E-mail: houjinxin_email@yeah.net

[†]E-mail: cxyue@lnnu.edu.cn

the $U(1)_{L_\mu-L_\tau}$ model is that the anomaly cancellation does not require any extra chiral fermionic degrees of freedom. In this model, the breaking of $L_\mu - L_\tau$ symmetry conduces to additional terms in the neutrino mass matrix, which offer an explanation for the neutrino masses and mixing simultaneously [34, 35]. Besides, the scalar sector has been expanded by two additional complex scalar singlets (ϕ_H and ϕ_{DM}) with nonzero $L_\mu - L_\tau$ charge. The scalar ϕ_{DM} can act as a viable DM candidate [36]. The other scalar ϕ_H acquires a vacuum expectation value (VEV) $v_{\mu\tau}$ and thereby making an additional neutral scalar h_2 product after spontaneous breaking of $U(1)_{L_\mu-L_\tau}$, which indicates that h_2 has a mass of the same order with $v_{\mu\tau}$ about 10 GeV - 1000 GeV [33, 37]. Owing to the significance of precise measurement of Higgs boson properties, many people are sparing no effort to search for the additional neutral scalars which can be produced and decay via their mixing with the SM-like Higgs boson h_1 [47].

On the other hand, an extra neutral gauge boson $Z_{\mu\tau}$ is also introduced and obtains a mass after spontaneous symmetry breaking of $U(1)_{L_\mu-L_\tau}$. $Z_{\mu\tau}$ does not couple to the SM quarks and the first generation leptons, which makes it immune to any restrictions coming from lepton and hadron colliders such as LEP and LHC. Therefore, the mass of $Z_{\mu\tau}$ can be as light as 100 MeV for a low value of gauge coupling $g_{\mu\tau} \leq 10^{-3}$, which is required to meet the limits arising from neutrino trident production. The $Z_{\mu\tau}$ with an MeV-scale mass can resolve the muon ($g-2$) anomaly, explain the deficit of cosmic neutrino flux [34, 39, 40] and resolve the problem of relic abundance of DM in the scenario with a light weakly interacting massive particle [41–43] simultaneously. Therefore, searching for its possible collider evidences plays a vital role in exploring NP. Many attempts to discover this kind of new particles have been made in the meson decay experiment [44], beam dump experiment [45], electron-positron collider experiments [46] and so on.

Searches for the new particles predicted by the $U(1)_{L_\mu-L_\tau}$ model are presently being conducted at the LHC and ILC [33]. While, another Higgs factory besides the LHC and ILC, such as the LHeC (Large Hadron electron Collider) and FCC-eh (Future Circular Collider in hadron-electron mode) [47–49], could precisely determine their specific properties. In this paper, we mainly devote to the study of the h_2 and $Z_{\mu\tau}$ productions and further explore the possibility of detecting their signatures at e-p colliders. We present a full simulation study of the production cross sections of h_2 and $Z_{\mu\tau}$ with the beam polarization $P(e^-) = -0.8$. Then, we investigate their observability through the $e^-p \rightarrow e^-j h_2 (\rightarrow Z_{\mu\tau} Z_{\mu\tau}) \rightarrow e^-j + \cancel{E}_T$ and $e^-p \rightarrow e^-j h_1 (\rightarrow Z_{\mu\tau} Z_{\mu\tau}) \rightarrow e^-j + \cancel{E}_T$ channels. We further analyze the signal significance of h_2 and $Z_{\mu\tau}$ detecting which depends on the model variables. Our numerical results show that the signals are promising to be detected at e-p colliders with appropriate parameter values and high integrated luminosity.

Rest of the paper has been arranged in the following manner. In Sec. II, we briefly review the basic features of the $U(1)_{L_\mu-L_\tau}$ model and show the allowed parameter space of this model. In Sec. III, we not only give the partial widths of major decay channels of the scalar h_2 , but also calculate its production cross sections via the W^+W^- and ZZ fusion processes. The production cross sections of the new gauge boson $Z_{\mu\tau}$ through h_2 and h_1 decays are calculated in Sec. IV. It is followed by a section on the phenomenology of the collider search, in which we estimate the numbers of the signal and background events, and investigate the signal observability and discovery potentiality of h_2 and $Z_{\mu\tau}$ through their respective promising production channels in Sec. V. Finally, our conclusions are given in Sec. VI.

II. The Basic Features of the $U(1)_{L_\mu-L_\tau}$ Model

The gauged $U(1)_{L_\mu-L_\tau}$ extension of the SM is one of the most extensively studied NP models, which can successfully solve the three major problems currently beyond the SM: the origin of tiny neutrino masses, the DM relic abundance and the muon $(g-2)$ anomalous magnetic moment. Refs. [34, 35] have made a detailed analysis about solving the above puzzles by using the $U(1)_{L_\mu-L_\tau}$ model. In this model, the gauge sector of the SM is enhanced by imposing a local $U(1)_{L_\mu-L_\tau}$ symmetry to the SM Lagrangian, where L_μ and L_τ are the muon and tau lepton numbers, respectively. Therefore, the complete gauged group is $SU(3)_C \times SU(2)_L \times U(1)_Y \times U(1)_{L_\mu-L_\tau}$. The SM particle content has been extended by including three extra right-handed (RH) neutrinos and two SM gauge singlet scalars. All particles included in the $U(1)_{L_\mu-L_\tau}$ model and their charge assignments under various symmetry groups are listed in Table 1.

Table 1: All particles and corresponding charge assignments under various symmetry groups in the $U(1)_{L_\mu-L_\tau}$ model.

Gauge Group	Scalar Fields			Lepton Fields								
	φ_h	φ_H	φ_{DM}	L_e	L_μ	L_τ	e_R	μ_R	τ_R	N_R^e	N_R^μ	N_R^τ
$SU(2)_L$	2	1	1	2	2	2	1	1	1	1	1	1
$U(1)_Y$	1/2	0	0	-1/2	-1/2	-1/2	-1	-1	-1	0	0	0
$U(1)_{L_\mu-L_\tau}$	0	1	$n_{\mu\tau}$	0	1	-1	0	1	-1	0	1	-1

Gauge Group	Baryon Fields											
	u_L	d_L	c_L	s_L	t_L	b_L	u_R	d_R	c_R	s_R	t_R	b_R
$SU(2)_L$	2	2	2	2	2	2	1	1	1	1	1	1
$U(1)_Y$	1/6	1/6	1/6	1/6	1/6	1/6	2/3	-1/3	2/3	-1/3	2/3	-1/3
$U(1)_{L_\mu-L_\tau}$	0	0	0	0	0	0	0	0	0	0	0	0

The complete Lagrangian for the $U(1)_{L_\mu-L_\tau}$ model is as follows

$$\mathcal{L} = \mathcal{L}_{SM} + \mathcal{L}_N + \mathcal{L}_{DM} + |D_\nu \varphi_H|^2 - V - \frac{1}{4} F_{\mu\tau}^{\rho\sigma} F_{\mu\tau\rho\sigma}. \quad (1)$$

The term \mathcal{L}_{SM} , \mathcal{L}_N and \mathcal{L}_{DM} represent the SM, right hand (RH) neutrino and DM sectors, respectively. Since the processes we are studying do not involve DM and RH neutrinos, the specific forms of their lagrangian descriptions are not given here. In Eq. (1), the covariant derivatives involving in the kinetic energy term $|D_\nu \varphi_H|^2$ of the extra Higgs singlet φ_H can be expressed in a generic form $D_\nu \phi = (\partial_\nu + i g_{\mu\tau} Q_{\mu\tau}(\phi) Z_{\mu\tau\nu}) \phi$, where ϕ is any SM single field which has $U(1)_{L_\mu-L_\tau}$ charge $Q_{\mu\tau}(\phi)$ (listed in Table 1) and $g_{\mu\tau}$ represents $U(1)_{L_\mu-L_\tau}$ group's gauge coupling constant. The scalar potential V contains all the self interactions of ϕ_H and its interactions with SM Higgs doublet. Its expression form is given by

$$V = \mu_H^2 \varphi_H^\dagger \varphi_H + \lambda_H (\varphi_H^\dagger \varphi_H)^2 + \lambda_{hH} (\varphi_h^\dagger \varphi_h) (\varphi_H^\dagger \varphi_H), \quad (2)$$

where the interactions of φ_H with φ_h are proportional to the coupling λ_{hH} . The last term in Eq. (1) represents the kinetic term for the additional gauge boson $Z_{\mu\tau}$ in terms with field

strength tensor $F_{\mu\tau}^{\rho\sigma} = \partial^\rho Z_{\mu\tau}^\sigma - \partial^\sigma Z_{\mu\tau}^\rho$ of the $U(1)_{L_\mu-L_\tau}$ gauge group. When the scalar field φ_H has a non-zero VEV, the $U(1)_{L_\mu-L_\tau}$ symmetry breaks spontaneously and consequently the corresponding new gauge boson $Z_{\mu\tau}$ acquires the mass $M_{Z_{\mu\tau}} = g_{\mu\tau} v_{\mu\tau}$. The SM Higgs doublet φ_h and the new scalar φ_H take the following form

$$\varphi_h = \begin{pmatrix} \tilde{H} \\ \frac{v+H+ia}{\sqrt{2}} \end{pmatrix}, \quad \varphi_H = \begin{pmatrix} \frac{v_{\mu\tau}+H_{\mu\tau}+ia}{\sqrt{2}} \end{pmatrix}, \quad (3)$$

where \tilde{H} , A and a are the massless Nambu-Goldstone Bosons (NGBs) absorbed by the gauge bosons W^+ , Z and $Z_{\mu\tau}$, while v and $v_{\mu\tau}$ are the VEVs of the scalars φ_h and φ_H , respectively. Furthermore, H and $H_{\mu\tau}$ represent the physical CP-even scalar bosons. When both φ_h and φ_H obtain their respective VEVs, there will be a mass mixing between the states H and $H_{\mu\tau}$. The square of scalar mass matrix with off-diagonal elements proportional to λ_{hH} is given by

$$\mathcal{M}_{scalar}^2 = \begin{pmatrix} 2\lambda_h v^2 & \lambda_{hH} v_{\mu\tau} v \\ \lambda_{hH} v_{\mu\tau} v & 2\lambda_H v_{\mu\tau}^2 \end{pmatrix}. \quad (4)$$

Rotating the basis states H and $H_{\mu\tau}$ by a suitable angle α , we can make the above mass matrix diagonal. The new basis states (h_1 and h_2), now representing two physical states, are the linear combinations of H and $H_{\mu\tau}$ with the mixing angle α between H and $H_{\mu\tau}$, which can be expressed as

$$h_1 = H \cos \alpha + H_{\mu\tau} \sin \alpha, \quad h_2 = -H \sin \alpha + H_{\mu\tau} \cos \alpha, \quad (5)$$

$$\tan 2\alpha = \frac{\lambda_{hH} v_{\mu\tau} v}{\lambda_h v^2 - \lambda_H v_{\mu\tau}^2}. \quad (6)$$

When $\alpha \ll 1$, h_1 can be identified as the SM-like Higgs boson which has already been discovered by the CMS [1] and ATLAS [2] collaborations in 2012. h_2 is playing the role of a new scalar particle. The masses of these two physical scalars h_1 and h_2 are given by

$$\begin{aligned} M_{h_1}^2 &= \sqrt{v^2 v_{\mu\tau}^2 (\lambda_{hH}^2 - 2\lambda_h \lambda_H) + \lambda_h^2 v^4 + \lambda_H^2 v_{\mu\tau}^4 + \lambda_h v^2 + \lambda_H v_{\mu\tau}^2}, \\ M_{h_2}^2 &= -\sqrt{v^2 v_{\mu\tau}^2 (\lambda_{hH}^2 - 2\lambda_h \lambda_H) + \lambda_h^2 v^4 + \lambda_H^2 v_{\mu\tau}^4 + \lambda_h v^2 + \lambda_H v_{\mu\tau}^2}. \end{aligned} \quad (7)$$

In this paper, we will assume that the values of M_{h_1} and v are fixed at 125 GeV and 246 GeV, respectively.

On one hand, compared with the SM Higgs boson, the couplings of h_1 with the SM particles are suppressed by the factor $\cos \alpha$ in the $U(1)_{L_\mu-L_\tau}$ model. Some relevant couplings of the new scalar h_1 and the new gauge boson $Z_{\mu\tau}$ with the SM particles are given by

$$g_{Z_{\mu\tau} Z_{\mu\tau} h_1} = \frac{2M_{Z_{\mu\tau}}^2}{v_{\mu\tau}} \sin \alpha, \quad g_{f\bar{f}h_1} = -\frac{M_f}{v} \cos \alpha, \quad g_{V V h_1} = \frac{2M_V^2}{v} \cos \alpha, \quad (8)$$

where f represents all of the SM fermions and V represents the electroweak gauge bosons W^\pm or Z . On the other hand, similar with h_1 , the scalar h_2 can couple to all the SM particles

and other new particles, such as new gauge boson $Z_{\mu\tau}$. Here, we also list the h_2 couplings, which are related our calculation

$$\begin{aligned} g_{Z_{\mu\tau}Z_{\mu\tau}h_2} &= \frac{2M_{Z_{\mu\tau}}^2}{v_{\mu\tau}} \cos \alpha, \quad g_{f\bar{f}h_2} = \frac{M_f}{v} \sin \alpha, \quad g_{VVh_2} = -\frac{2M_V^2}{v} \sin \alpha, \\ g_{h_1h_1h_2} &= 6v\lambda_{h_1} \cos^2 \alpha \sin \alpha - 6v_{\mu\tau}\lambda_{h_2} \sin^2 \alpha \cos \alpha - 2v\lambda_{h_1h_2} \sin \alpha + 6v\lambda_{h_1h_2} \sin^3 \alpha \\ &\quad - v_{\mu\tau}\lambda_{h_1h_2} \cos \alpha + 3v_{\mu\tau}\lambda_{h_1h_2} \sin^2 \alpha \cos \alpha. \end{aligned} \quad (9)$$

In the $U(1)_{L_\mu-L_\tau}$ model, $Z_{\mu\tau}$ has a light mass and no couplings to the SM quarks and the first generation leptons, so it can only decay to neutrinos. The couplings of $Z_{\mu\tau}$ with neutrinos are expressed as

$$g_{Z_{\mu\tau}v_\mu v_\mu} = \frac{M_{Z_{\mu\tau}}}{v_{\mu\tau}}, \quad g_{Z_{\mu\tau}v_\tau v_\tau} = -\frac{M_{Z_{\mu\tau}}}{v_{\mu\tau}}. \quad (10)$$

Taking no account of the neutrino masses, the expression form of the total decay width of $Z_{\mu\tau}$ is given by

$$\Gamma_{Z_{\mu\tau}} = \frac{g_{\mu\tau}^2 M_{Z_{\mu\tau}}}{12\pi}, \quad (11)$$

where we have also ignored the neutrino mixing.

To produce the appropriate neutrino mass and explain the muon ($g-2$) anomaly, Ref. [33] has show the favored regions of the gauge coupling $g_{\mu\tau}$ and the $Z_{\mu\tau}$ mass, which are summarized as

$$g_{\mu\tau} \simeq [2 \times 10^{-4}, 2 \times 10^{-3}], \quad M_{Z_{\mu\tau}} \simeq [5, 210] \text{ MeV}. \quad (12)$$

According to Eq. (12), the window of $v_{\mu\tau}$ is given by

$$v_{\mu\tau} = \frac{M_{Z_{\mu\tau}}}{g_{\mu\tau}} \simeq [10, 1000] \text{ GeV}, \quad (13)$$

which indicates that, after the spontaneous symmetry breaking, the new scalar h_2 have a mass of the same order with $v_{\mu\tau}$. Furthermore, using the constraint on the branching ratio of the Higgs invisible decay, $\text{BR}_{\text{invis}} \leq 0.24$ at 95% C. L. from the LHC data [50], the sine of scalar mixing angle $\sin \alpha$ must be satisfied $\sin \alpha \leq 0.3$. Then, for the factor χ , there is

$$\chi = \frac{\alpha}{v_{\mu\tau}} \leq 2.2 \times 10^{-4} \text{ GeV}^{-1}. \quad (14)$$

To summarize, in the $U(1)_{L_\mu-L_\tau}$ model, three free parameters are newly introduced, which are the new gauge coupling constant $g_{\mu\tau}$, the $Z_{\mu\tau}$ mass $M_{Z_{\mu\tau}}$ and the scalar mixing angle α , respectively. In the following, we will focus our attention on the unique phenomenology of the new particles h_2 and $Z_{\mu\tau}$ with the above allowed parameter space.

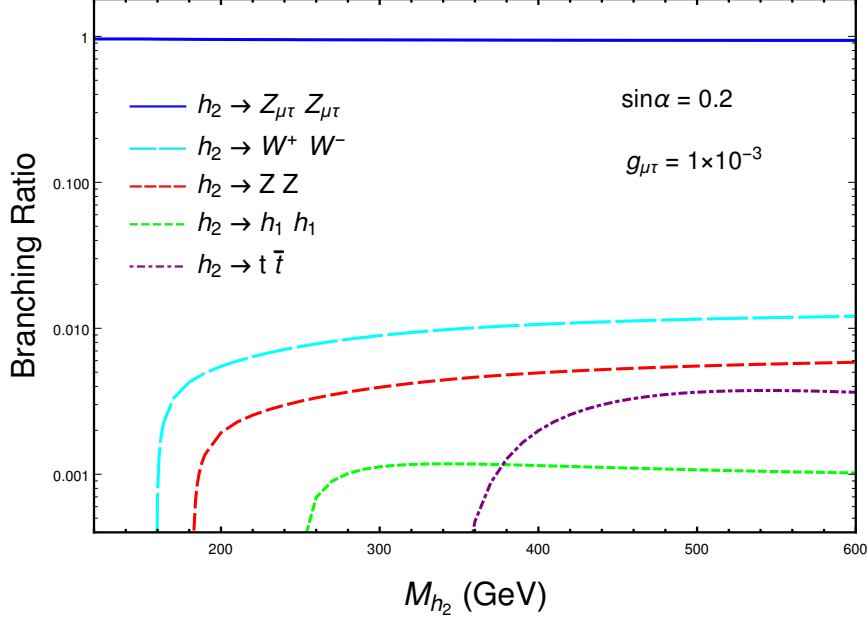


Figure 1: The branching ratios for the main decay modes of the scalar h_2 as functions of M_{h_2} for the fixed values $\sin\alpha = 0.2$ and $g_{\mu\tau} = 1 \times 10^{-3}$.

III. Decays and Productions of the Scalar h_2

3.1. Decays of the scalar h_2

In the $U(1)_{L_\mu-L_\tau}$ model, the additional scalar h_2 can not only decay to the SM particles but also decay to $Z_{\mu\tau}$. Here, we give the decay width expressions of its several major decay modes. The expression form of the decay width for the decay channel $h_2 \rightarrow Z_{\mu\tau}Z_{\mu\tau}$ is given by

$$\Gamma(h_2 \rightarrow Z_{\mu\tau}Z_{\mu\tau}) = \frac{g_{h_2 Z_{\mu\tau} Z_{\mu\tau}}^2 (M_{h_2}^4 - 4M_{Z_{\mu\tau}}^2 M_{h_2}^2 + 12M_{Z_{\mu\tau}}^2) \sqrt{M_{h_2}^2 - 4M_{Z_{\mu\tau}}^2}}{128\pi M_{h_2}^2 M_{Z_{\mu\tau}}^4}. \quad (15)$$

Under the assumption $\frac{M_{Z_{\mu\tau}}}{M_{h_1}} \rightarrow 0$, we can obtain the following form

$$\Gamma(h_2 \rightarrow Z_{\mu\tau}Z_{\mu\tau}) = \frac{M_{h_2}^3 \cos^2 \alpha}{32\pi v_{\mu\tau}^2}. \quad (16)$$

The width of h_2 decaying to vector bosons is given as follows

$$\Gamma(h_2 \rightarrow VV) = \frac{g_{h_2 VV}^2 (M_{h_2}^4 - 4M_V^2 M_{h_2}^2 + 12M_V^2) \sqrt{M_{h_2}^2 - 4M_V^2}}{64\pi S_V M_{h_2}^2 M_V^4}, \quad (17)$$

where S_V represents the statistical factor. Its value equals to 1 for W^\pm boson and 2 for Z boson. The width for the decay process $h_2 \rightarrow h_1 h_1$ can be written as

$$\Gamma(h_2 \rightarrow h_1 h_1) = \frac{g_{h_1 h_1 h_2}^2 \sqrt{M_{h_2}^2 - 4M_{h_1}^2}}{32\pi M_{h_2}^2} . \quad (18)$$

The width of h_2 decaying to the SM fermion pair is given as follows

$$\Gamma(h_2 \rightarrow f\bar{f}) = \frac{n_c g_{h_2 f f} (M_{h_2}^2 - 4M_f^2)^{\frac{3}{2}}}{8\pi M_{h_2}^2} , \quad (19)$$

where the color charge $n_c = 1$ for leptons and 3 for quarks. Fig. 1 shows the branching ratios for the main decay modes of the scalar h_2 as functions of the mass parameter M_{h_2} for the fixed values $\sin\alpha = 0.2$ and $g_{\mu\tau} = 1 \times 10^{-3}$, where the curves from high to low correspond the $Z_{\mu\tau}Z_{\mu\tau}$ decay modes, the W^+W^-/ZZ decay modes, di-higgs decay mode and di-top decay mode, respectively. One can see from this figure that the value of the branching ratio $BR(h_2 \rightarrow Z_{\mu\tau}Z_{\mu\tau})$ is about 98% and only is 2% for the rest decay channels. Certainly, the values of these branching ratios would vary as the values of the parameters $\sin\alpha$ and $g_{\mu\tau}$ changing. However, in the allowed parameter space of the $U(1)_{L_\mu-L_\tau}$ model, the decay process $h_2 \rightarrow Z_{\mu\tau}Z_{\mu\tau}$ is the main decay channel of the scalar h_2 . So, we will choose it to study the feasibility of detecting h_2 at e-p colliders.

3.2. Productions of the scalar h_2

Like the SM Higgs boson, the additional scalar h_2 in the $U(1)_{L_\mu-L_\tau}$ model is produced via two major channels: the charged current (CC) production channel via W^+W^- fusion and the neutral current (NC) production channel via ZZ fusion [51, 52] at e-p colliders. Fig. 2 gives the corresponding Feynman diagrams for the h_2 production via CC production channel and NC production channel at e-p colliders, respectively. Then, employing

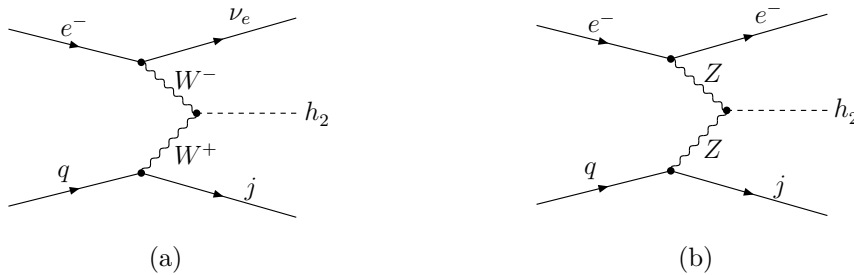


Figure 2: The Feynman diagrams for the scalar h_2 productions at e-p colliders (Left (a): CC production channel, Right (b): NC production channel).

Madgraph5/aMC@NLO [53], we calculate the production cross sections of the processes $e^-p \rightarrow \nu_e j h_2$ and $e^-p \rightarrow e^- j h_2$ as functions of $M_{Z_{\mu\tau}}$ at the LHeC. It is well known that polarization of the initial state electron can affect the production cross sections. Our numerical results show that the beam polarization $P(e^-) = -0.8$ can maximize the cross sections. Therefore, we will take $P(e^-) = -0.8$ in following numerical calculation. Since $g_{\mu\tau}$ does not affect the cross sections of h_2 production via the CC and NC processes, we do

not consider it here. In Figs. 3 (a) and 3 (b), the curves show the cross sections of the $e^-p \rightarrow e^-jh_2$ and $e^-p \rightarrow \nu_ejh_2$ processes with $E_e = 140$ GeV and different values of mixing angle $\sin\alpha = 0.2$ (solid), 0.05 (dashed) and 0.01 (dotted). One can see from these figures that the values of the production cross section σ decrease as the h_2 mass increases. For the $e^-p \rightarrow e^-jh_2$ process and $10 \text{ GeV} \leq M_{h_2} \leq 1000 \text{ GeV}$, its values are in the ranges of $1.73 \text{ pb} \times 10^{-6} \leq \sigma \leq 4.33 \times 10^{-3} \text{ pb}$ (solid), $1.08 \times 10^{-7} \text{ pb} \leq \sigma \leq 2.71 \times 10^{-4} \text{ pb}$ (dashed) and $4.33 \times 10^{-9} \text{ pb} \leq \sigma \leq 1.08 \times 10^{-5} \text{ pb}$ (dotted), respectively. For the $e^-p \rightarrow \nu_ejh_2$ process and $10 \text{ GeV} \leq M_{h_2} \leq 1000 \text{ GeV}$, its values are in the ranges of $1.77 \times 10^{-5} \text{ pb} \leq \sigma \leq 3.73 \times 10^{-2} \text{ pb}$ (solid), $1.11 \times 10^{-6} \text{ pb} \leq \sigma \leq 2.33 \times 10^{-3} \text{ pb}$ (dashed) and $4.43 \times 10^{-8} \text{ pb} \leq \sigma \leq 9.32 \times 10^{-5} \text{ pb}$ (dotted) respectively. It is worth mentioning that the cross section of the $e^-p \rightarrow \nu_ejh_2$ process is larger than that of the $e^-p \rightarrow e^-jh_2$ process by about one order of magnitude.

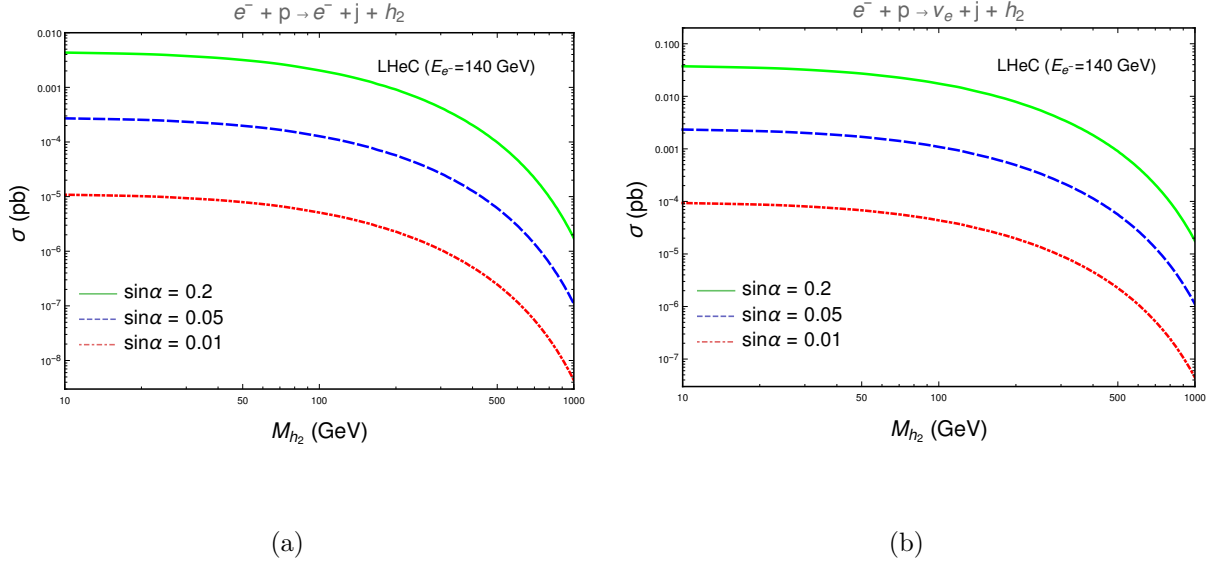


Figure 3: The production cross sections of the processes $e^-p \rightarrow e^-jh_2$ and $e^-p \rightarrow \nu_ejh_2$ as functions of the mass parameter M_{h_2} for $\sin\alpha = 0.2$ (solid), 0.05 (dashed), 0.01 (dotted) and the beam polarization $P(e^-) = -0.8$ at the LHeC.

IV. Productions of the New Gauge Boson $Z_{\mu\tau}$

Now, we turn our attention to $Z_{\mu\tau}$. As mentioned in the previous section, $Z_{\mu\tau}$ can not establish couplings with all the SM quarks and the first generation leptons, making it very difficult to be produced directly. So it is a very attractive scheme to obtain $Z_{\mu\tau}$ by considering its indirect production. Similar with the new scalar h_2 , besides decaying to the SM particles, the SM-like Higgs boson h_1 can also decay to a pair of $Z_{\mu\tau}$. The decay width is given by

$$\Gamma(h_1 \rightarrow Z_{\mu\tau}Z_{\mu\tau}) = \frac{g_{h_1Z_{\mu\tau}Z_{\mu\tau}}^2 (M_{h_1}^4 - 4M_{Z_{\mu\tau}}^2 M_{h_1}^2 + 12M_{Z_{\mu\tau}}^2) \sqrt{M_{h_1}^2 - 4M_{Z_{\mu\tau}}^2}}{128\pi M_{h_1}^2 M_{Z_{\mu\tau}}^4}, \quad (20)$$

which can be simplified to

$$\Gamma(h_1 \rightarrow Z_{\mu\tau} Z_{\mu\tau}) = \frac{M_{h_1}^3 \sin^2 \alpha}{32\pi v_{\mu\tau}^2} . \quad (21)$$

From above equation we can see that the production rate of the $Z_{\mu\tau}$ pair from h_1 decaying is actually determined by the factor $\chi^2 \simeq \sin^2 \alpha / v_{\mu\tau}^2$. So, in this work, all the results for the $Z_{\mu\tau}$ production via h_1 decaying can be expressed as functions of the factor χ . Next, we will consider the indirect productions of $Z_{\mu\tau}$ via the decays of h_2 and h_1 , respectively.

As can be seen from Fig. 3, the CC production of scalar h_2 has larger cross section than that for its NC production. For this reason, we choose the CC production channels of h_2 and h_1 to study the $Z_{\mu\tau}$ productions. However, as mentioned earlier, $Z_{\mu\tau}$ can only decay to neutrinos in the $U(1)_{L_\mu-L_\tau}$ model. So the final states of the $e^-p \rightarrow \nu_e j h_2 (h_2 \rightarrow Z_{\mu\tau} Z_{\mu\tau})$ and $e^-p \rightarrow \nu_e j h_1 (h_1 \rightarrow Z_{\mu\tau} Z_{\mu\tau})$ processes would be jets and missing energy, which are difficult to be distinguished from the deeply inelastic scattering (DIS) background. Moreover, lack of kinematic handles in the final state makes it extremely difficult to filter signal from many backgrounds. Therefore, in this work we will focus on the NC production channels $e^-p \rightarrow e^- j h_1 (\rightarrow Z_{\mu\tau} Z_{\mu\tau}) \rightarrow e^- j + \cancel{E}_T$ and $e^-p \rightarrow e^- j h_2 (\rightarrow Z_{\mu\tau} Z_{\mu\tau}) \rightarrow e^- j + \cancel{E}_T$ to study the feasibility of detecting h_2 and $Z_{\mu\tau}$. In Fig. 4, we show the leading order Feynman diagrams of the $Z_{\mu\tau}$ productions by the decays of h_1 and h_2 via the NC production channel at e-p colliders.

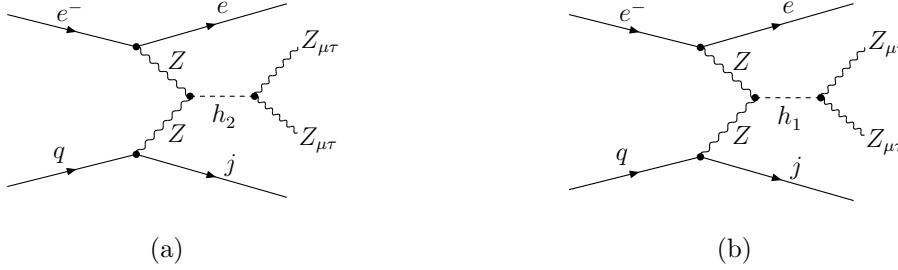


Figure 4: The Feynman diagrams of the $Z_{\mu\tau}$ productions by the decays of h_1 and h_2 via the NC production channel at e-p colliders.

Then, employing the Madgraph5/aMC@NLO [53], we calculate the cross sections of the $Z_{\mu\tau}$ production processes $e^-p \rightarrow e^- j h_2 \rightarrow e^- j Z_{\mu\tau} Z_{\mu\tau}$ and $e^-p \rightarrow e^- j h_1 \rightarrow e^- j Z_{\mu\tau} Z_{\mu\tau}$. Considering the favored region of the parameter space to resolve $(g-2)_\mu$ discrepancy, $g_{\mu\tau}$ is fixed to $g_{\mu\tau} = 1 \times 10^{-3}$ for reference. Fig. 5 (a) displays the cross sections of the $Z_{\mu\tau}$ production via h_2 decaying as functions of the mass M_{h_2} for $\sin \alpha = 0.2$ (solid), 0.05 (dashed) and 0.01 (dotted) at LHeC with $E_{e^-} = 140$ GeV. Fig. 5 (b) shows the cross sections of the $Z_{\mu\tau}$ production by h_1 decaying as functions of the factor χ at e-p colliders, where the different curves show the $Z_{\mu\tau}$ production cross sections at different colliders: FCC-eh (solid), LHeC with $E_{e^-} = 140$ GeV (dashed) and LHeC with $E_{e^-} = 60$ GeV (dotted). From Fig. 5 (a), we can see that the values of σ decrease as $M_{Z_{\mu\tau}}$ increases. For $g_{\mu\tau} = 1 \times 10^{-3}$ and 10 GeV $\leq M_{Z_{\mu\tau}} \leq 1000$ GeV, its values are in the ranges 1.15×10^{-6} pb $\leq \sigma \leq 4.30 \times 10^{-3}$ pb (solid), 7.25×10^{-8} pb $\leq \sigma \leq 2.69 \times 10^{-4}$ pb (dashed) and 2.90×10^{-9} pb $\leq \sigma \leq 1.08 \times 10^{-5}$ pb (dotted), respectively. From Fig. 5 (b), we can see that, for 1×10^{-5} GeV $\leq \chi \leq 2 \times 10^{-4}$ GeV, the values of the $Z_{\mu\tau}$ production cross sections are in the ranges

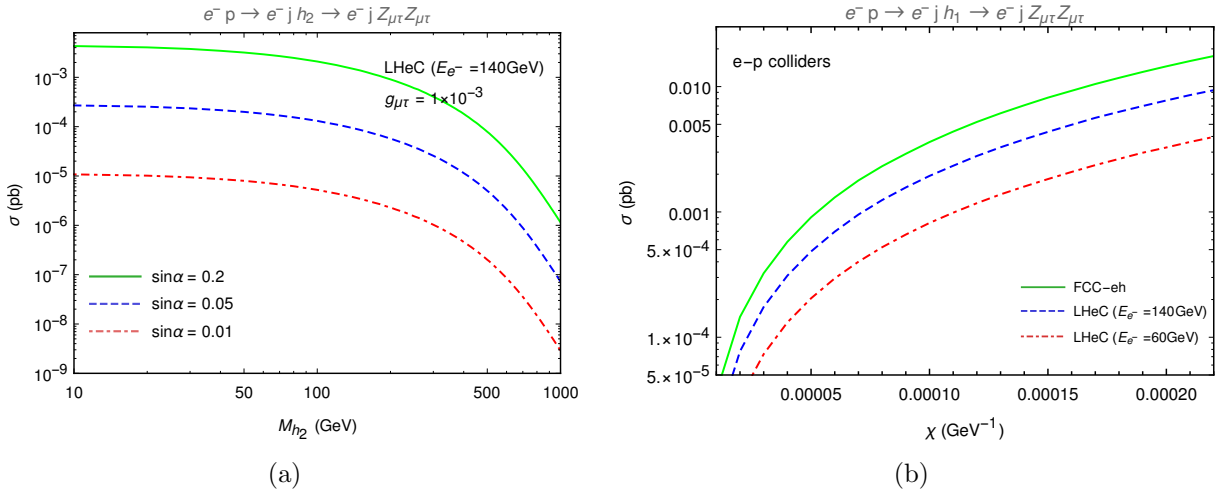


Figure 5: (a) The production cross sections of the process $e^-p \rightarrow e^-j h_2 \rightarrow e^-j Z_{\mu\tau} Z_{\mu\tau}$ as functions of M_{h_2} with different values of $\sin\alpha$ for $g_{\mu\tau} = 1 \times 10^{-3}$ and $M_{Z_{\mu\tau}} = 0.1$ GeV at the LHeC with $E_{e^-} = 140$ GeV. (b) The production cross sections of the process $e^-p \rightarrow e^-j h_1 \rightarrow e^-j Z_{\mu\tau} Z_{\mu\tau}$ as functions of χ at e-p colliders.

3.61×10^{-5} pb $\leq \sigma \leq 1.75 \times 10^{-2}$ pb (solid), 1.94×10^{-5} pb $\leq \sigma \leq 9.37 \times 10^{-3}$ pb (dashed) and 8.16×10^{-6} pb $\leq \sigma \leq 3.97 \times 10^{-3}$ pb (dotted), which correspond FCC-eh, LHeC with $E_{e^-} = 140$ GeV and LHeC with $E_{e^-} = 60$ GeV, respectively.

V. Signatures of the new particles h_2 and $Z_{\mu\tau}$ at e-p Colliders

In this section, we analyze the observation potential by performing a Monte Carlo simulation of the signal and background events and explore the observability of the additional scalar h_2 and the new gauge boson $Z_{\mu\tau}$ at e-p colliders with the integrated luminosity of 1 ab^{-1} . The following is organized as follows: On one hand, we explore the observability of h_2 as well as $Z_{\mu\tau}$ via $e^-p \rightarrow e^-j h_2 \rightarrow e^-j Z_{\mu\tau} Z_{\mu\tau}$ process. On the other hand, we will analyse the $e^-p \rightarrow e^-j h_1 \rightarrow e^-j Z_{\mu\tau} Z_{\mu\tau}$ process aiming at exploring the signature of $Z_{\mu\tau}$.

We use Madgraph5/aMC@NLO [53] to calculate the relevant production cross sections and generate the signal and background events, where the UFO format of the $U(1)_{L_\mu-L_\tau}$ model has been obtained by using FeynRules [54]. Moreover, the parton distribution function (PDF), NNPDF2.3 [55], is used at leading order and Pythia-pgs [56] is employed for parton showering, hadronization and fast detector simulation. Finally, MadAnalysis5 [57] is applied for data analysis and plotting. All of the SM input parameters are taken from Particle Data Group (PDG) [58].

In this section, we take both h_2 and h_1 productions at e-p colliders through CC production channels followed by $h_2 \rightarrow Z_{\mu\tau} Z_{\mu\tau}$ and $h_1 \rightarrow Z_{\mu\tau} Z_{\mu\tau}$ as our signals, signal-1 and signal-2, respectively. Since $Z_{\mu\tau}$ has invisible final state in the detector, these two processes provide the same final state that includes one electron, one jet and a large missing transverse energy \cancel{E}_T

$$e^- + p \rightarrow e^- + j + h_2 (\rightarrow Z_{\mu\tau} Z_{\mu\tau}) \rightarrow e^- + j + \cancel{E}_T, \text{ (signal - 1)} \quad (22)$$

$$e^- + p \rightarrow e^- + j + h_1(\rightarrow Z_{\mu\tau}Z_{\mu\tau}) \rightarrow e^- + j + \cancel{E}_T, \text{ (signal-2)} \quad (23)$$

in which \cancel{E}_T comes from $Z_{\mu\tau} \rightarrow \nu\bar{\nu}$. For $\sin\alpha = 0.2$ and $g_{\mu\tau} = 1 \times 10^{-3}$, the values of the cross section for the signal-1 are 4.179×10^{-4} pb (1.046×10^{-4} pb) for $E_{e^-} = 140$ (60) GeV at the LHeC and 9.251×10^{-4} pb at the FCC-eh. While the values of the cross section for the signal-2 are 1.898×10^{-3} pb (5.441×10^{-4} pb) for $E_{e^-} = 140$ (60) GeV at the LHeC and 2.412×10^{-3} pb at the FCC-eh for $\chi = 9 \times 10^{-5}$ GeV $^{-1}$.

For the signal $e^-j\cancel{E}_T$, the leading irreducible SM backgrounds can be classified into two general categories. The first category has a final state $e^-j\nu_e\bar{\nu}_e$ which comes from the following two processes

$$e^- + p \rightarrow W^-(\rightarrow e^-\bar{\nu}_e) + j + \nu_e \rightarrow e^- + j + \cancel{E}_T, (e^-j\nu_e\bar{\nu}_e) \quad (24)$$

$$e^- + p \rightarrow Z(\rightarrow \nu_e\bar{\nu}_e) + j + e^- \rightarrow e^- + j + \cancel{E}_T. (e^-j\nu_e\bar{\nu}_e) \quad (25)$$

The total cross section for this kind of irreducible backgrounds is 0.4334 pb (0.205 pb) for $E_{e^-} = 140$ (60) GeV at the LHeC and 0.8116 pb at the FCC-eh, which will severely pollute the physical signal.

The second category has a final state $e^-j\nu_{\mu,\tau}\bar{\nu}_{\mu,\tau}$

$$e^- + p \rightarrow Z(\rightarrow \nu_{\mu,\tau}\bar{\nu}_{\mu,\tau}) + j + e^- \rightarrow e^- + j + \cancel{E}_T. (e^-j\nu_{\mu,\tau}\bar{\nu}_{\mu,\tau}) \quad (26)$$

Its production cross section is 0.05685 pb (0.03422 pb) for $E_{e^-} = 140$ (60) GeV at the LHeC and 0.1052 pb at the FCC-eh. Besides, more remarkably, the photoproduction of the state $W+j$, which has a larger cross section, is also an irreducible SM background if the W boson decays to an electron and neutrino. But it can be negligible after all selection cuts, because of its unique kinematic features.

There are also some reducible backgrounds which come from various sources. The most threatening reducible backgrounds result from the production of τ in the final state. One is

$$e^- + p \rightarrow e^- + j + \tau^+ + \nu_\tau. (e^-j\tau^+\nu_\tau) \quad (27)$$

Its cross section is 0.264 pb (0.1331 pb) for $E_{e^-} = 140$ (60) GeV at the LHeC and 0.3957 pb at the FCC-eh. The other one is

$$e^- + p \rightarrow e^- + j + \tau^- + \bar{\nu}_\tau. (e^-j\tau^-\bar{\nu}_\tau) \quad (28)$$

Its cross section is 0.2816 pb (0.1362 pb) for $E_{e^-} = 140$ (60) GeV at the LHeC and 0.5015 pb at the FCC-eh. The main reasons why the above two processes (Eq. (27) and Eq. (28)) can be viewed as reducible backgrounds are: (I) The τ -jets may be misidentified as hadronic jets. (II) The detection of hadronic decay products of τ cannot be expected to be fully efficient due to the products being too soft, which will lead to generation of the missing energy \cancel{E}_T . Furthermore, we can even consider the case (II) as a source of partial irreducible background. The $e^-p \rightarrow \nu_e j \tau^+ \nu_\tau$ and $e^-p \rightarrow \nu_e j \tau^- \bar{\nu}_\tau$ processes are reducible backgrounds in which the τ decays to an electron. Fortunately, we could suppress them to an insignificant order because of the totally different kinematic distribution of the final electron. Some other reducible backgrounds are e +multijet productions in which the \cancel{E}_T comes from jet's mismeasurement and $jj\nu$ production in which one jet is misidentified as an electron. In this work, we do not simulate both of them because their contributions can be negligible after all

selection cuts. The signal and background events are generated with following basic cuts [51] in Madgraph5/aMC@NLO [53]

- lepton transverse momentum $p_T(l^\pm) > 5$ GeV,
- jet transverse momentum $p_T(j) > 20$ GeV,
- lepton pseudorapidity in the range $|\eta(l^\pm)| < 5$,
- jet pseudorapidity in the range $|\eta(j)| < 5$,
- angular separation between jet and lepton $\Delta R(jl^\pm) > 0.4$,

where $\eta = 1/2 \ln(\tan \theta)$ is the pseudorapidity, where θ indicates the scattering angle in the laboratory frame. $\Delta R = \sqrt{(\Delta\phi)^2 + (\Delta\eta)^2}$ is the particle separation, where $\Delta\phi$ and $\Delta\eta$ represent the rapidity gap and the azimuthal angle gap between the particle pair, respectively.

Table 2: Effect of individual kinematical cuts on the signal-1 for $M_{h_2} = 300$ GeV, $M_{Z_{\mu\tau}} = 0.1$ GeV, $\sin\alpha = 0.2$ and $g_{\mu\tau} = 1 \times 10^{-3}$, and the SM backgrounds at the LHeC with $E_{e^-} = 140$ (60) GeV. The statistical significance is computed for the integrated luminosity as 1 ab^{-1} .

LHeC,	$E_{e^-} = 140$ (60) GeV,	$E_p = 7$ TeV	
cuts	signal (S)	total background (B)	$S/\sqrt{S+B}$
initial (no cut)	417.0 (104.0)	1.01×10^6 (5.09×10^5)	0.41 (0.15)
basic cuts	392.1 (97.6)	8.53×10^5 (4.11×10^5)	0.42 (0.16)
$\cancel{E}_T < 20$ ($\cancel{E}_T < 20$) GeV	238.6 (70.7)	5.17×10^4 (4.89×10^4)	1.05 (0.32)
TET > 300 (TET > 260) GeV	235.9 (64.6)	1.65×10^4 (4.63×10^3)	1.83 (0.94)
THT > 200 (THT > 200) GeV	235.7 (63.8)	9.91×10^3 (1.42×10^3)	2.30 (1.65)
$E_T(jj) > 100$ ($E_T(jj) > 90$) GeV	232.7 (60.4)	7.83×10^3 (1.08×10^3)	2.59 (1.79)
$E_T(e^-j) > 150$ ($E_T(e^-j) > 120$) GeV	232.3 (59.5)	7.44×10^3 (9.93×10^2)	2.65 (1.84)

Table 3: Effect of individual kinematical cuts on the signal-2 for $M_{h_1} = 125$ GeV, $M_{Z_{\mu\tau}} = 0.1$ GeV and $\chi = 9 \times 10^{-5} \text{ GeV}^{-1}$, and the SM backgrounds at the LHeC with $E_{e^-} = 140$ (60) GeV. The statistical significance is computed for the integrated luminosity as 1 ab^{-1} .

LHeC,	$E_{e^-} = 140$ (60) GeV,	$E_p = 7$ TeV	
cuts	signal (S)	total background (B)	$S/\sqrt{S+B}$
initial (no cut)	1288.0 (544.0)	1.01×10^6 (5.09×10^5)	1.28 (0.76)
basic cuts	1205.9 (508.1)	8.53×10^5 (4.11×10^5)	1.30 (0.79)
$\cancel{E}_T < 20$ ($\cancel{E}_T < 18$) GeV	980.9 (386.0)	8.79×10^4 (4.05×10^4)	3.29 (1.91)
TET > 200 (TET > 160) GeV	827.7 (361.9)	2.26×10^4 (1.27×10^4)	5.41 (3.16)
THT > 140 (THT > 120) GeV	808.1 (354.3)	1.20×10^4 (6.09×10^3)	7.14 (4.41)
$E_T(jj) > 60$ ($E_T(jj) > 60$) GeV	803.5 (374.8)	9.65×10^3 (4.46×10^3)	7.86 (5.02)
$E_T(e^-j) > 100$ ($E_T(e^-j) > 80$) GeV	796.1 (343.7)	8.96×10^3 (4.19×10^3)	8.06 (5.10)

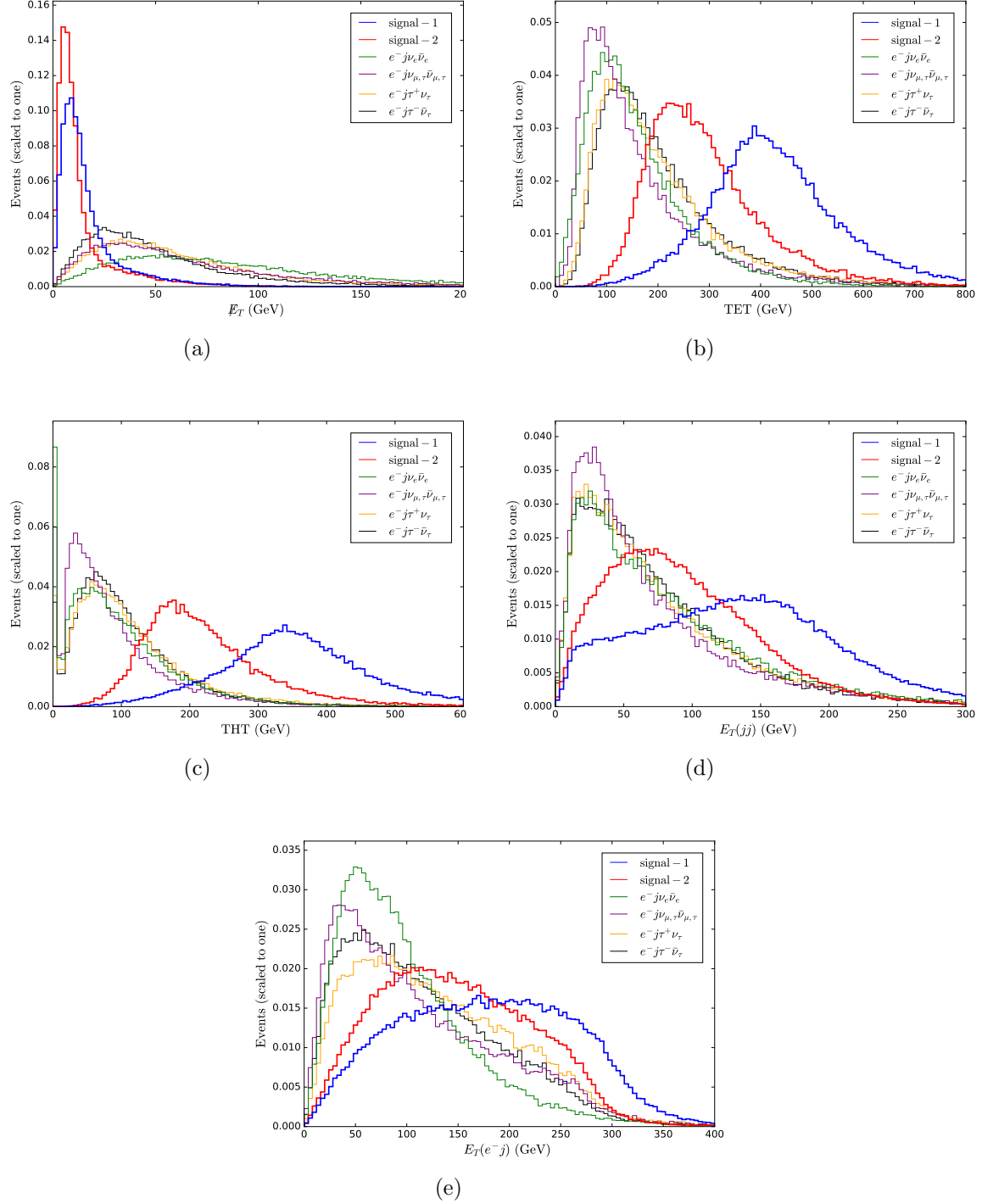


Figure 6: Normalized distributions of \cancel{E}_T (a), TET (b), THT (c), $E_T(jj)$ (d) and $E_T(e^-j)$ (e) for the signals and backgrounds at the LHeC with $E_{e^-} = 140$ GeV and an integrated luminosity of 1 ab^{-1} .

After the basic cuts, we further employ optimized kinematical cuts on separating the signals from the SM backgrounds. In our theoretical framework, although the SM backgrounds have a huge effect on the signals, there are many kinematical differences between them that can be exploited. In Fig. 6, we show the normalized distributions of the total missing transverse energy \cancel{E}_T , the visible transverse energy TET, the missing transverse hadronic energy THT, jet pair transverse energy $E_T(jj)$ and electron jet transverse energy $E_T(e^-j)$ for the signals and backgrounds at the LHeC with $E_{e^-} = 140$ GeV and an integrated luminosity of 1 ab^{-1} . From this figure, we can see that the distributions of signals have good distinctions from the distributions of the relevant backgrounds (peaks locate in different locations). In principle, there are other variables which we can use to discriminate the signals from backgrounds. But, these variables are remarkably similar and can not work significantly better than above kinematic variables. After all these kinematical cuts are applied, the event numbers of signal-1, signal-2 and corresponding backgrounds are summarized in Table 2 and Table 3 for the LHeC with $E_{e^-} = 140$ (60) GeV, respectively. The values of the statistical significance SS are also shown in these tables, which is defined as $SS = S/\sqrt{S+B}$ with S and B being the number of signal and background events, respectively.

Table 4: Effect of individual kinematical cuts on the signal-1 for $M_{h_2} = 300$ GeV, $M_{Z_{\mu\tau}} = 0.1$ GeV, $\sin\alpha = 0.2$ and $g_{\mu\tau} = 1 \times 10^{-3}$ and backgrounds at the FCC-eh. The statistical significance SS is computed for an integrated luminosity of 1 ab^{-1} .

FCC-eh,	$E_{e^-} = 60$ GeV,	$E_p = 50$ TeV	
cuts	signal (S)	total background (B)	$S/\sqrt{S+B}$
initial (no cut)	925.0	1.81×10^6	0.69
basic cuts	863.3	1.30×10^6	0.76
$\cancel{E}_T < 20$ GeV	303.2	1.29×10^5	0.84
TET > 280 GeV	279.1	1.35×10^4	2.38
THT > 200 GeV	277.7	7.34×10^3	3.18
$E_T(jj) > 100$ GeV	263.7	5.84×10^3	3.38
$E_T(e^-j) > 120$ GeV	261.9	5.61×10^3	3.42

Table 5: Effect of individual kinematical cuts on the signal-2 for $M_{h_1} = 125$ GeV, $M_{Z_{\mu\tau}} = 0.1$ GeV and $\chi = 9 \times 10^{-5} \text{ GeV}^{-1}$ and backgrounds at the FCC-eh. The statistical significance SS is computed for an integrated luminosity of 1 ab^{-1} .

FCC-eh,	$E_{e^-} = 60$ GeV,	$E_p = 50$ TeV	
cuts	signal (S)	total background (B)	$S/\sqrt{S+B}$
initial (no cut)	2412.0	1.82×10^6	1.79
basic cuts	2246.7	1.30×10^6	1.96
$\cancel{E}_T < 20$ GeV	1086.9	1.29×10^5	3.01
TET > 180 GeV	981.0	3.76×10^4	5.00
THT > 120 GeV	972.0	2.46×10^4	6.08
$E_T(jj) > 60$ GeV	959.3	1.92×10^4	6.76
$E_T(e^-j) > 80$ GeV	952.9	1.79×10^4	6.94

On the other hand, it is well known that the FCC-eh collides electrons to protons with $E_{e^-} = 60$ GeV and $E_p = 50$ TeV, which is a typical deep inelastic facility with $\sqrt{s} \approx 3.5$

TeV. Therefore, we need to modify the above veto criteria and kinematic cuts to adjust the progressive detector simulation, because the FCC-eh has a higher proton beam energy than LHeC. The modified values for the kinematic cuts and the event numbers of signal-1, signal-2 and backgrounds are presented in Table 4 and Table 5, respectively.

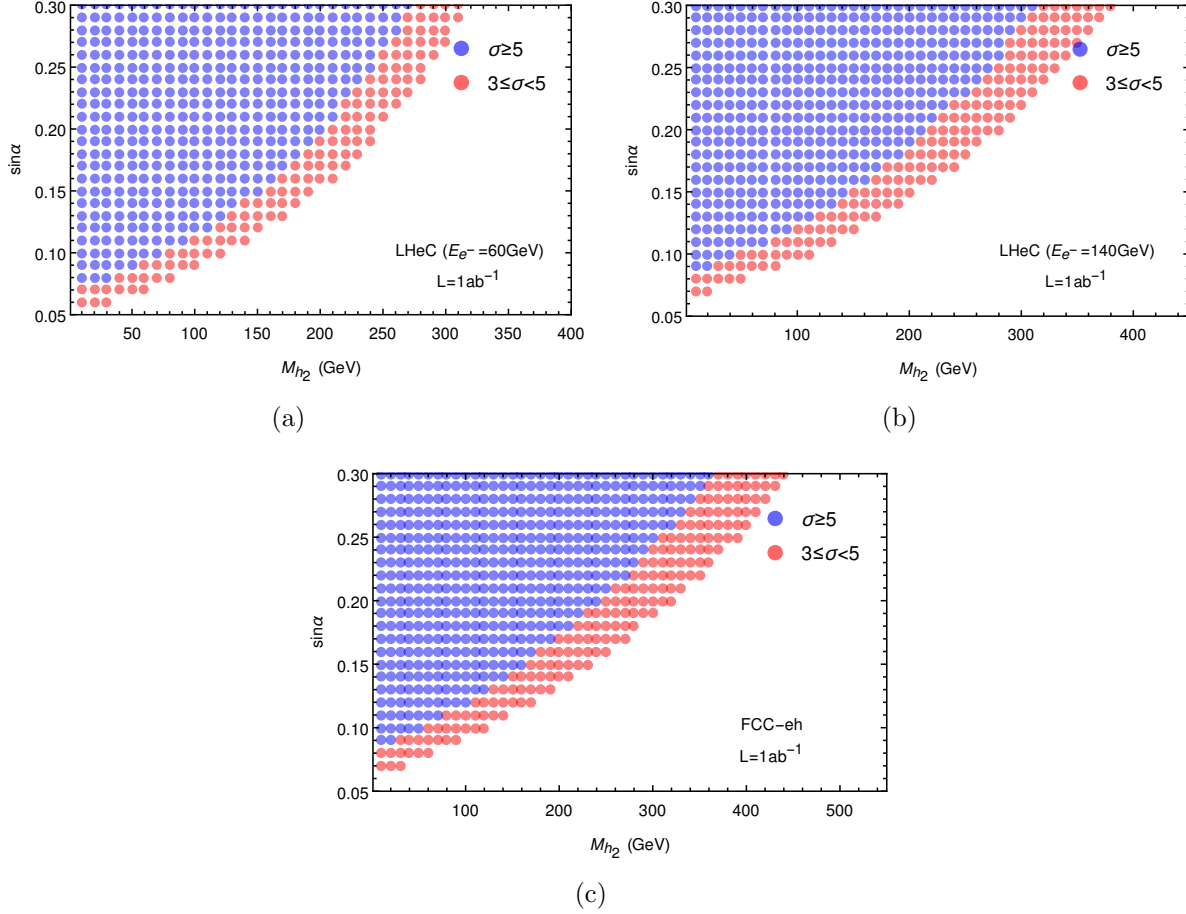


Figure 7: 3σ and 5σ detection potential regions for the signal-1 at the LHeC with $E_{e^-} = 60$ GeV (a), LHeC with $E_{e^-} = 140$ GeV (b) and FCC-eh (c) with an integrated luminosity of 1 ab^{-1} , respectively.

From these tables, we can see that, for $\sin \alpha = 0.2$, $M_{Z_{\mu\tau}} = 0.1$ GeV, $M_{h_2} = 300$ GeV, $g_{\mu\tau} = 1 \times 10^{-3}$ and the integrated luminosity being 1 ab^{-1} , the values of SS for signal-1 can reach 2.65 (1.84) at the LHeC with $E_{e^-} = 140$ (60) GeV and 3.42 at the FCC-eh with $E_{e^-} = 60$ GeV, $E_p = 50$ TeV. The values of SS for signal-2 can reach 8.06 (5.10) at the LHeC with $E_{e^-} = 140$ (60) GeV and 6.94 at the FCC-eh with $E_{e^-} = 60$ GeV, $E_p = 50$ TeV when we take $M_{Z_{\mu\tau}} = 0.1$ GeV, $\chi = 9 \times 10^{-5} \text{ GeV}^{-1}$ and an integrated luminosity of 1 ab^{-1} .

In Figs. 7 (a), 7 (b) and 7 (c), performing the scan over the parameter spaces of M_{h_2} and $\sin \alpha$ for $M_{Z_{\mu\tau}} = 0.1$ GeV, we show the experimental evidence region ($3 \leq SS < 5$) and experimental discovery region ($5 \leq SS$) of signal-1 at different e-p colliders with integrated luminosity being 1 ab^{-1} . For $\sin \alpha \leq 0.3$, from Fig. 7 (a), we obtain the h_2 mass region of above 3σ confidence level as $10 \text{ GeV} \leq M_{h_2} \leq 320 \text{ GeV}$ and above 5σ confidence level as $10 \text{ GeV} \leq M_{h_2} \leq 270 \text{ GeV}$ at the LHeC with $E_{e^-} = 60$ GeV. From Fig. 7 (b), we obtain the h_2 mass region of above 3σ confidence level as $10 \text{ GeV} \leq M_{h_2} \leq 400 \text{ GeV}$ and above 5σ confidence level as $10 \text{ GeV} \leq M_{h_2} \leq 310 \text{ GeV}$ at the LHeC with $E_{e^-} = 140$ GeV. From Fig. 7 (c), we obtain the h_2 mass region of above 3σ confidence level as $10 \text{ GeV} \leq M_{h_2} \leq 480 \text{ GeV}$

and above 5σ confidence level as $10 \text{ GeV} \leq M_{h_2} \leq 360 \text{ GeV}$ at the FCC-eh. Based on these numerical results, we can say that the possible signatures of h_2 and $Z_{\mu\tau}$ from signal-1 is limited in the lower M_{h_2} range and could be detected at e-p colliders with an integrated luminosity of 1 ab^{-1} . On the other side, the FCC-eh could offer a better detection capabilities than LHeC under the same integrated luminosity.

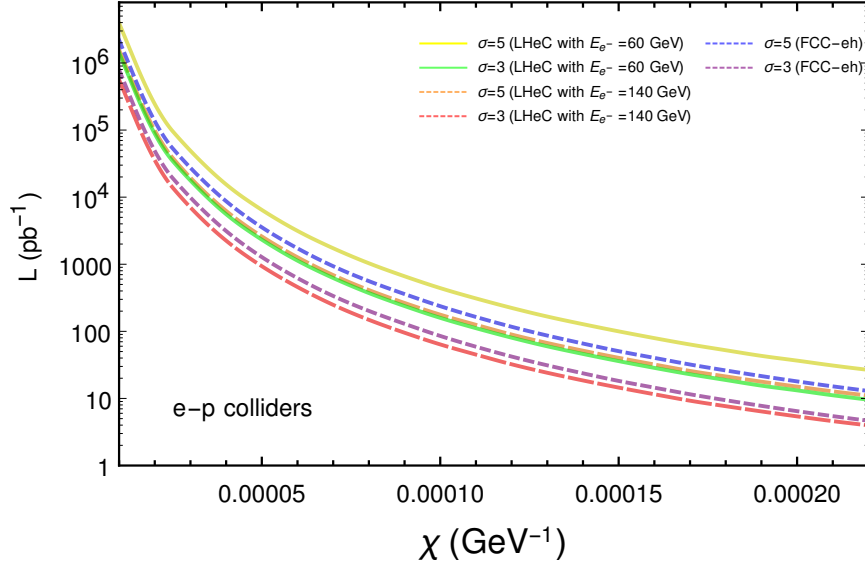


Figure 8: Integrated luminosity required for observing the signal-2 at the 3σ and 5σ statistical significance at different values of χ at e-p colliders.

The required integrated luminosities for observing the new gauge boson $Z_{\mu\tau}$ from signal-2 at the 3σ and 5σ confidence levels at different e-p colliders are plotted as functions of χ in Fig. 8. We can see that one can obtain larger statistical significance for larger χ value within allowed parameter space from Fig. 8. We can easily obtain 5σ statistical significance for taking $\chi \geq 5 \times 10^{-5}$ within the designed luminosity region. In addition, by contrast, the LHeC with $E_{e^-} = 140 \text{ GeV}$ has the best sensitivity to the signal-2. Thus, from a phenomenological point of view, the signal-2 is more likely to result in a detection of the new gauge boson $Z_{\mu\tau}$ at a lower integrated luminosity and more achievable experimental conditions.

VI. Conclusions

The $U(1)_{L_\mu-L_\tau}$ model, which can explain the muon $(g-2)$ anomaly, small neutrino masses and provide a candidate of DM, is phenomenologically rich and predictive. In this model, the additional scalar h_2 and gauge boson $Z_{\mu\tau}$ are obtained after spontaneous breaking of $L_\mu - L_\tau$ symmetry. New scalar h_2 mixing with the SM-like Higgs boson is helpful to improve the precision of Higgs boson measurements. Furthermore, the gauge boson $Z_{\mu\tau}$ possessing a mass around the MeV scale can explain the deficit of cosmic neutrino flux and resolve the problem of muon $(g-2)$ anomaly and relic abundance of DM simultaneously. So, studying these two new particles is of great significance for exploring this kind of new physics models. In this paper, we have studied the possibility of searching for the new particles h_2 and $Z_{\mu\tau}$ at e-p colliders. Since $Z_{\mu\tau}$ can not couple with the SM quarks and the

first generation leptons, it is very difficult to be produced directly at colliders. So we consider its productions via decays of h_1 and h_2 . Although the CC production of h_1 and h_2 have larger cross sections, their final states will generate mono-jet plus missing energy, which accidentally coincides with the DIS backgrounds. Therefore we focus on NC production channels $e^-p \rightarrow e^-j h_1(\rightarrow Z_{\mu\tau} Z_{\mu\tau}) \rightarrow e^-j + \cancel{E}_T$ and $e^-p \rightarrow e^-j h_2(\rightarrow Z_{\mu\tau} Z_{\mu\tau}) \rightarrow e^-j + \cancel{E}_T$, which provide good kinematic handles to distinguish the signals from the SM backgrounds.

After giving the decay width expressions of several main decay channels of new scalar h_2 , we calculate the production cross sections of the processes $e^-p \rightarrow e^-j h_2$ and $e^-p \rightarrow \nu_e j h_2$ with the beam polarization $P(e^-) = -0.8$ in the context of the $U(1)_{L_\mu-L_\tau}$ model. Then, the production cross sections of $Z_{\mu\tau}$ are further calculated. Then, we investigate the observability of h_2 and $Z_{\mu\tau}$ through the signal-1 from the process $e^-p \rightarrow e^-j h_2(\rightarrow Z_{\mu\tau} Z_{\mu\tau}) \rightarrow e^-j + \cancel{E}_T$ and the signal-2 from the process $e^-p \rightarrow e^-j h_1(\rightarrow Z_{\mu\tau} Z_{\mu\tau}) \rightarrow e^-j + \cancel{E}_T$ at e-p colliders with 1 ab^{-1} integrated luminosity. After simulating the signals as well as the relevant backgrounds, and applying suitable kinematic cuts on the variables \cancel{E}_T , TET, THT, $E_T(jj)$ and $E_T(e^-j)$, the values of the statistical significance SS for signal-1 can reach 2.65 (1.84) at the LHeC with $E_{e^-} = 140$ (60) GeV and 3.42 at the FCC-eh with $E_{e^-} = 60$ GeV, $E_p = 50$ TeV when we take $\sin\alpha = 0.2$, $g_{\mu\tau} = 1 \times 10^{-3}$ GeV, $M_{Z_{\mu\tau}} = 0.1$ GeV and $M_{h_2} = 300$ GeV. While for signal-2, its values can reach 8.06 (5.10) at the LHeC with $E_{e^-} = 140$ (60) GeV and 6.94 at the FCC-eh when we take $\chi = 9 \times 10^{-5}$ GeV^{-1} and $M_{Z_{\mu\tau}} = 0.1$ GeV. Performing the scan over all parameter space, we find that the signature of h_2 and $Z_{\mu\tau}$ from signal-1 is limited in the lower M_{h_2} range and could be detected at e-p colliders with an integrated luminosity of 1 ab^{-1} . On the other side, the FCC-eh could offer better detection capabilities than LHeC under the same integrated luminosity. In addition, our numerical results show that the signature of $Z_{\mu\tau}$ might be easily detected via signal-2 at e-p colliders and the LHeC with $E_{e^-} = 140$ GeV has the best sensitivity to signal-2. Thus, we expect that the signatures of the $U(1)_{L_\mu-L_\tau}$ model might be detected at future e-p colliders.

ACKNOWLEDGEMENT

This work was supported in part by the National Natural Science Foundation of China under Grant Nos.11875157, 11847303 and 11605081.

References

- [1] G. Aad *et al.* [ATLAS Collaboration], “Observation of a new particle in the search for the Standard Model Higgs boson with the ATLAS detector at the LHC,” Phys. Lett. B **716**, 1 (2012) [arXiv:1207.7214 [hep-ex]].
- [2] S. Chatrchyan *et al.* [CMS Collaboration], “Observation of a new boson at a mass of 125 GeV with the CMS experiment at the LHC,” Phys. Lett. B **716**, 30 (2012) [arXiv:1207.7235 [hep-ex]].
- [3] Y. Fukuda *et al.* [Super-Kamiokande Collaboration], “Evidence for oscillation of atmospheric neutrinos,” Phys. Rev. Lett. **81**, 1562 (1998) [hep-ex/9807003].

- [4] Q. R. Ahmad *et al.* [SNO Collaboration], “Measurement of the rate of $\nu_e + d \rightarrow p + p + e^-$ interactions produced by 8B solar neutrinos at the Sudbury Neutrino Observatory,” *Phys. Rev. Lett.* **87**, 071301 (2001) [nucl-ex/0106015].
- [5] P. A. R. Ade *et al.* [Planck Collaboration], “Planck 2013 results. XVI. Cosmological parameters,” *Astron. Astrophys.* **571**, A16 (2014) [arXiv:1303.5076 [astro-ph.CO]].
- [6] G. Bertone, D. Hooper and J. Silk, “Particle dark matter: Evidence, candidates and constraints,” *Phys. Rept.* **405**, 279 (2005) [hep-ph/0404175].
- [7] S. Perlmutter *et al.* [Supernova Cosmology Project Collaboration], “Measurements of Omega and Lambda from 42 high redshift supernovae,” *Astrophys. J.* **517**, 565 (1999) [astro-ph/9812133].
- [8] A. G. Riess *et al.* [Supernova Search Team], “Observational evidence from supernovae for an accelerating universe and a cosmological constant,” *Astron. J.* **116**, 1009 (1998) [astro-ph/9805201].
- [9] O. Cakir, A. Senol and A. T. Tasci, “Single Production of Fourth Family t-prime Quarks at LHeC,” *EPL* **88**, no. 1, 11002 (2009) [arXiv:0905.4347 [hep-ph]].
- [10] H. Liang, X. G. He, W. G. Ma, S. M. Wang and R. Y. Zhang, “Seesaw Type I and III at the LHeC,” *JHEP* **1009**, 023 (2010) [arXiv:1006.5534 [hep-ph]].
- [11] Z. Zhang [LHeC Study Group], “Top and EW Physics at the LHeC,” *PoS EPS - HEP2015*, 342 (2015) [arXiv:1511.05399 [hep-ex]].
- [12] S. Antusch, E. Cazzato and O. Fischer, “Sterile neutrino searches at future e^-e^+ , pp , and e^-p colliders,” *Int. J. Mod. Phys. A* **32**, no. 14, 1750078 (2017) [arXiv:1612.02728 [hep-ph]].
- [13] D. Curtin, K. Deshpande, O. Fischer and J. Zurita, “New Physics Opportunities for Long-Lived Particles at Electron-Proton Colliders,” *JHEP* **1807**, 024 (2018) [arXiv:1712.07135 [hep-ph]].
- [14] W. R. Porod, “SUSY overview,” *PoS ALPS* **2018**, 024 (2018).
- [15] F. Carta, S. Giacomelli and R. Savelli, “SUSY enhancement from T-branes,” *JHEP* **1812**, 127 (2018) [arXiv:1809.04906 [hep-th]].
- [16] J. Mamuzic [ATLAS Collaboration], “Recent SUSY results in ATLAS,” *PoS CORFU* **2017**, 060 (2018).
- [17] N. Kitazawa, “Brane SUSY Breaking and the Gravitino Mass,” *JHEP* **1804**, 081 (2018) [arXiv:1802.03088 [hep-th]].
- [18] K. S. Babu and S. Jana, “Enhanced Di-Higgs Production in the Two Higgs Doublet Model,” *JHEP* **1902**, 193 (2019) [arXiv:1812.11943 [hep-ph]].
- [19] T. Kon, T. Nagura, T. Ueda and K. Yagyu, “Double Higgs boson production at e^+e^- colliders in the two-Higgs-doublet model,” [arXiv:1812.09843 [hep-ph]].

- [20] S. K. Kang, Z. Qian, J. Song and Y. W. Yoon, “Confronting the fourth generation two Higgs doublet model with the phenomenology of heavy Higgs bosons,” *Phys. Rev. D* **98**, no. 9, 095025 (2018) [arXiv:1810.05229 [hep-ph]].
- [21] P. Chaber, B. Dziewit, J. Holeczek, M. Richter, M. Zralek and S. Zajac, “Lepton masses and mixing in a two-Higgs-doublet model,” *Phys. Rev. D* **98**, no. 5, 055007 (2018) [arXiv:1808.08384 [hep-ph]].
- [22] S. P. Li, X. Q. Li and Y. D. Yang, “Muon $g-2$ in a $U(1)$ -symmetric Two-Higgs-Doublet Model,” *Phys. Rev. D* **99**, no. 3, 035010 (2019) [arXiv:1808.02424 [hep-ph]].
- [23] D. Azevedo, P. Ferreira, M. M. Mühlleitner, R. Santos and J. Wittbrodt, “Models with extended Higgs sectors at future e^+e^- colliders,” *Phys. Rev. D* **99**, no. 5, 055013 (2019) [arXiv:1808.00755 [hep-ph]].
- [24] K. Asai, K. Hamaguchi, N. Nagata, S. Y. Tseng and K. Tsumura, “Minimal Gauged $U(1)_{L_\alpha-L_\beta}$ Models Driven into a Corner,” *Phys. Rev. D* **99**, no. 5, 055029 (2019) [arXiv:1811.07571 [hep-ph]].
- [25] B. C. Allanach, J. Davighi and S. Melville, “An Anomaly-free Atlas: charting the space of flavour-dependent gauged $U(1)$ extensions of the Standard Model,” *JHEP* **1902**, 082 (2019) [arXiv:1812.04602 [hep-ph]].
- [26] G. Chauhan, P. S. B. Dev, R. N. Mohapatra and Y. Zhang, “Perturbativity constraints on $U(1)_{B-L}$ and left-right models and implications for heavy gauge boson searches,” *JHEP* **1901**, 208 (2019) [arXiv:1811.08789 [hep-ph]].
- [27] L. Delle Rose, S. Khalil, S. J. D. King, S. Moretti and A. M. Thabt, “Atomki Anomaly in Family-Dependent $U(1)'$ Extension of the Standard Model,” *Phys. Rev. D* **99**, no. 5, 055022 (2019) [arXiv:1811.07953 [hep-ph]].
- [28] X. G. He, G. C. Joshi, H. Lew and R. R. Volkas, “Simplest Z-prime model,” *Phys. Rev. D* **44**, 2118 (1991).
- [29] X. G. He, G. C. Joshi, H. Lew and R. R. Volkas, “NEW Z-prime PHENOMENOLOGY,” *Phys. Rev. D* **43**, 22 (1991).
- [30] M. Drees, M. Shi and Z. Zhang, “Constraints on $U(1)_{L_\mu-L_\tau}$ from LHC Data,” *Phys. Lett. B* **791**, 130 (2019) [arXiv:1811.12446 [hep-ph]].
- [31] J. X. Hou, C. X. Yue and Z. H. Zhao, “Detecting the light gauge boson $Z_{\mu\tau}$ via Higgsstrahlung process in the $U(1)_{L_\mu-L_\tau}$ model at e^+e^- colliders,” *Nucl. Phys. B* **940**, 377 (2019).
- [32] H. Banerjee and S. Roy, “Signatures of supersymmetry and $L_\mu - L_\tau$ gauge bosons at Belle-II,” *Phys. Rev. D* **99**, no. 3, 035035 (2019) [arXiv:1811.00407 [hep-ph]].
- [33] T. Nomura and T. Shimomura, “Light Z' boson from scalar boson decay at collider experiments in an $U(1)_{L_\mu-L_\tau}$ model,” [arXiv:1803.00842 [hep-ph]].
- [34] A. Biswas, S. Choubey and S. Khan, “FIMP and Muon $(g-2)$ in a $U(1)_{L_\mu-L_\tau}$ Model,” *JHEP* **1702**, 123 (2017) [arXiv:1612.03067 [hep-ph]].

- [35] A. Biswas, S. Choubey and S. Khan, “Neutrino Mass, Dark Matter and Anomalous Magnetic Moment of Muon in a $U(1)_{L_\mu-L_\tau}$ Model,” JHEP **1609**, 147 (2016) [arXiv:1608.04194 [hep-ph]].
- [36] T. Araki, S. Hoshino, T. Ota, J. Sato and T. Shimomura, “Detecting the $L_\mu - L_\tau$ gauge boson at Belle II,” Phys. Rev. D **95**, no. 5, 055006 (2017) [arXiv:1702.01497 [hep-ph]].
- [37] S. N. Gninenko and N. V. Krasnikov, “Probing the muon $g_\mu - 2$ anomaly, $L_\mu - L_\tau$ gauge boson and Dark Matter in dark photon experiments,” Phys. Lett. B **783**, 24 (2018) [arXiv:1801.10448 [hep-ph]].
- [38] L. Delle Rose, A. Hammad and O. Fischer, “Prospects for Heavy Scalar Searches at the LHeC,” [arXiv:1809.04321 [hep-ph]].
- [39] A. Kamada and H. B. Yu, “Coherent Propagation of PeV Neutrinos and the Dip in the Neutrino Spectrum at IceCube,” Phys. Rev. D **92**, no. 11, 113004 (2015) [arXiv:1504.00711 [hep-ph]].
- [40] T. Araki, F. Kaneko, T. Ota, J. Sato and T. Shimomura, “MeV scale leptonic force for cosmic neutrino spectrum and muon anomalous magnetic moment,” Phys. Rev. D **93**, no. 1, 013014 (2016) [arXiv:1508.07471 [hep-ph]].
- [41] S. Baek and P. Ko, “Phenomenology of $U(1)_{L(\mu)-L(\tau)}$ charged dark matter at PAMELA and colliders,” JCAP **0910**, 011 (2009) [arXiv:0811.1646 [hep-ph]].
- [42] S. Baek, “Dark matter and muon ($g-2$) in local $U(1)_{L_\mu-L_\tau}$ -extended Ma Model,” Phys. Lett. B **756**, 1 (2016) [arXiv:1510.02168 [hep-ph]].
- [43] S. Patra, S. Rao, N. Sahoo and N. Sahu, “Gauged $U(1)_{L_\mu-L_\tau}$ model in light of muon $g-2$ anomaly, neutrino mass and dark matter phenomenology,” Nucl. Phys. B **917**, 317 (2017) [arXiv:1607.04046 [hep-ph]].
- [44] D. Banerjee *et al.* [NA64 Collaboration], “Search for vector mediator of Dark Matter production in invisible decay mode,” Phys. Rev. D **97**, no. 7, 072002 (2018) [arXiv:1710.00971 [hep-ex]].
- [45] M. Anelli *et al.* [SHiP Collaboration], “A facility to Search for Hidden Particles (SHiP) at the CERN SPS,” [arXiv:1504.04956 [physics.ins-det]].
- [46] T. Abe *et al.* [Belle-II Collaboration], “Belle II Technical Design Report,” [arXiv:1011.0352 [physics.ins-det]].
- [47] L. Delle Rose, A. Hammad and O. Fischer, “Prospects for Heavy Scalar Searches at the LHeC,” [arXiv:1809.04321 [hep-ph]].
- [48] F. Bordry, M. Benedikt, O. Brüning, J. Jowett, L. Rossi, D. Schulte, S. Stapnes and F. Zimmermann, “Machine Parameters and Projected Luminosity Performance of Proposed Future Colliders at CERN,” [arXiv:1810.13022 [physics.acc-ph]].
- [49] C. Han, R. Li, R. Q. Pan and K. Wang, “Searching for the light Higgsinos in the MSSM at future e-p colliders,” Phys. Rev. D **98**, no. 11, 115003 (2018) [arXiv:1802.03679 [hep-ph]].

- [50] G. Aad, et al., [ATLAS Collaboration], Constraints on new phenomena via Higgs boson couplings and invisible decays with the ATLAS detector, JHEP **1511**, 206 (2015) [arXiv:1509.00672].
- [51] Y. L. Tang, C. Zhang and S. H. Zhu, “Invisible Higgs Decay at the LHeC,” Phys. Rev. D **94**, no. 1, 011702 (2016) [arXiv:1508.01095 [hep-ph]].
- [52] T. Han and B. Mellado, “Higgs Boson Searches and the H b anti-b Coupling at the LHeC,” Phys. Rev. D **82**, 016009 (2010) [arXiv:0909.2460 [hep-ph]].
- [53] J. Alwall *et al.*, “The automated computation of tree-level and next-to-leading order differential cross sections, and their matching to parton shower simulations,” JHEP **1407**, 079 (2014) [arXiv:1405.0301 [hep-ph]].
- [54] N. D. Christensen and C. Duhr, “FeynRules - Feynman rules made easy,” Comput. Phys. Commun. **180**, 1614 (2009) [arXiv:0806.4194 [hep-ph]].
- [55] R. D. Ball *et al.* [NNPDF Collaboration], “Parton distributions with QED corrections,” Nucl. Phys. B **877**, 290 (2013) [arXiv:1308.0598 [hep-ph]].
- [56] T. Sjostrand, S. Mrenna and P. Z. Skands, “PYTHIA 6.4 Physics and Manual,” JHEP **0605**, 026 (2006) [hep-ph/0603175].
- [57] E. Conte, B. Fuks and G. Serret, “MadAnalysis 5, A User-Friendly Framework for Collider Phenomenology,” Comput. Phys. Commun. **184**, 222 (2013) [arXiv:1206.1599 [hep-ph]].
- [58] M. Tanabashi *et al.* [Particle Data Group], “Review of Particle Physics,” Phys. Rev. D **98**, no. 3, 030001 (2018).